Published in final edited form as:
Science. 2014 October 3; 346(6205): 85–89. doi:10.1126/science.1250255.

Ubiquitylome analysis identifies dysregulation of effector substrates in SPOP-mutant prostate cancer

Jean-Philippe P. Theurillat[#1,2,3], **Namrata D. Udeshi**[#1], **Wesley J. Errington**[#4,5], **Tanya Svinkina**[1], **Sylvan C. Baca**[2,3], **Marius Pop**[1,2,3], **Peter J. Wild**[6], **Mirjam Blattner**[7], **Anna C. Groner**[3], **Mark A. Rubin**[7,8], **Holger Moch**[6], **Gilbert G. Prive**[4,5], **Steven A. Carr**[1], and **Levi A. Garraway**[1,2,3,9,*]

[1]The Broad Institute of Harvard and MIT, Cambridge, MA 02142, USA [2]Harvard Medical School, Boston, MA 02115, USA [3]Department of Medical Oncology, Dana-Farber Cancer Institute, Boston, MA 02115, USA [4]Department of Biochemistry, University of Toronto, Toronto, Ontario M5S 1A8, Canada [5]Princess Margaret Cancer Centre, University Health Network, Toronto, Ontario, M5G 2M9. Canada [6]Institute of Surgical Pathology, University Hospital Zurich, Zurich, ZH 8091, Switzerland [7]Department of Pathology and Laboratory Medicine, Weill Cornell Medical College, New York, NY 10065, USA [8]Institute for Precision Medicine of Weill Cornell and New York Presbyterian Hospital, New York, NY 10065 [9]Center for Cancer Genome Discovery, Dana-Farber Cancer Institute, Boston, MA 02115, USA

[#] These authors contributed equally to this work.

Abstract

Cancer genome characterization has revealed driver mutations in genes that govern ubiquitylation; however, the mechanisms by which these alterations promote tumorigenesis remain incompletely characterized. Here, we analyzed changes in the ubiquitin landscape induced by prostate cancer-associated mutations of SPOP, an E3 ubiquitin ligase substrate binding protein. SPOP mutants impaired ubiquitylation of a subset of proteins in a dominant-negative fashion. Of these, DEK and TRIM24 emerged as effector substrates consistently up-regulated by SPOP mutants. We highlight DEK as a SPOP substrate that exhibited decreases in ubiquitylation and proteasomal degradation resulting from heteromeric complexes of wild-type and mutant SPOP protein. DEK stabilization promoted prostate epithelial cell invasion, implicating DEK as an oncogenic effector. More generally, these results provide a framework to decipher tumorigenic mechanisms linked to dysregulated ubiquitylation.

Genome sequencing studies have revealed unanticipated roles for the ubiquitylation machinery in cancer. For example, the cullin-RING ubiquitin ligase adaptor protein speckle-

[*]Correspondence to: Levi_Garraway@dfci.harvard.edu.

Supplementary Materials:
Materials and Methods
Figures S1-S10
Tables S1-S3
References 24-30

type POZ protein (SPOP) is mutated in 8-14% of prostate and endometrial cancers (1-4). In prostate cancer, SPOP mutations are confined to specific amino acid residues within the substrate-binding cleft, which mediates substrate interaction and ubiquitin transfer (5). This exquisite localization suggests that SPOP mutations have undergone positive selection during tumorigenesis by altering binding and ubiquitylation of distinct effector substrates in a pro-tumorigenic manner. However, the mechanisms and substrates underlying this phenomenon remain incompletely understood.

In principle, mutant SPOP could enhance ubiquitylation of SPOP substrates (gain of function effect) or ubiquitylate new substrates (neomorphic effect). Alternatively, SPOP mutants could dimerize with their wild type counterparts (e.g., through the BTB and BACK domain), thereby repressing wild-type SPOP function (dominant-negative effect). In support of the latter model, SPOP mutations typically occur in a heterozygous state with a retained wild-type allele and are able to dysregulate known substrates (e.g., NCOA3) in a dominant-negative manner (6).

Characterizing the ubiquitin landscape (or “ubiquitylome”) that results from cancer genomic alterations affecting ubiquitin ligase components may provide new insights into tumorigenesis. To interrogate changes in ubiquitylation conferred by prostate cancer SPOP mutations, we stably over-expressed either vector control (C), wild type SPOP (SPOP-WT) or a mutated variant (SPOP-F133L or SPOP-Y87N; SPOP-MT) in immortalized prostate epithelial cells expressing endogenous SPOP (fig. S1A, B) (7). In each case, we characterized the resulting ubiquitylome by measuring glycine-glycine remnants of ubiquitylated lysines (K-ε-GG) after trypsin digestion and stable isotope labeling of amino acids in cell culture (SILAC)-based mass-spectrometry (MS) (Fig. 1A). To account for ubiquitylation-related changes in protein expression, all K-ε-GG values were normalized to protein abundance (Fig. 1A, database D1).

We reasoned that putative K-ε-GG peptide substrates might show distinct patterns of protein abundance depending on whether mutant SPOP caused a dominant-negative, loss-of-function, gain-of-function, or neomorphic effect. In a dominant negative context, substrate peptides should exhibit a [SPOP-WT > control > SPOP-MT] pattern of abundance, whereas a pure loss-of-function effect might yield a [SPOP-WT > control = SPOP-MT] pattern. In contrast, a gain-of-function effect may result in a [SPOP-MT > SPOP-WT > control] pattern, and a neomorphic effect should cause a [SPOP-MT > SPOP-WT = control] pattern.

Only 12 of 7181 K-ε-GG peptides detected exhibited >2-fold changes in peptide abundance in the SPOP-mutant contexts (Z-score >3 or <-3) compared to control or SPOP-WT (Fig. 1B, figs. S1C, D, table S1, database D1). Differentially regulated (>2-fold) K-ε-GG peptides generally followed a dominant-negative pattern, including those corresponding to WIZ, SCAF1, GLYR1, DEK and TRIM24 proteins (Fig. 1B, figs. S1C-D and S2A-E). K-ε-GG peptides from two proteins (corresponding to G3BP1 and CAPRIN1) showed a loss-of-function pattern (fig. S1C, D and S2F, G), and two K-ε-GG peptides from SPOP itself showed up-regulation in the setting of both SPOP-WT and SPOP-mutant overexpression, suggestive of auto-ubiquitylation (fig. S1C, D). Although we observed no evidence for gain-of-function or neomorphic effects, we cannot exclude the existence of such mechanisms.

We next determined whether SPOP binding motifs were enriched in the differentially regulated proteins. Indeed, of the seven proteins described above (excluding SPOP itself), three (43%) contained a previously characterized SPOP binding sequence (DEK, SCAF1 and CAPRIN1) (5). In contrast, the frequency of SPOP binding sites was significantly lower (~3%) across the ubiquitylome as a whole ($p < 0.001$; table S2). We identified one K-ε-GG peptide corresponding to DAXX, a known SPOP substrate (8). As expected, this peptide was enriched—and the corresponding total protein was down regulated—following overexpression of wild-type SPOP (fig. S3A). Expression of NCOA3, another SPOP substrate, followed a dominant-negative pattern as reported previously (6, 9) (fig. S3B).

Since protein ubiquitylation is often a prerequisite for proteasomal degradation, we next sought to ascertain which differentially expressed K-ε-GG peptides showed an inverse correlation with total protein expression (database D1). Peptides corresponding to TRIM24, SCAF1 and GLYR1 fit this pattern (1 peptide each; Fig. 1C, fig. S3C and D). TRIM24 has been shown to mediate ligand-dependent activation of the androgen receptor--a key prostate cancer driver–and to degrade TP53 through its E3 ligase activity (10, 11). This observation is of interest given that primary prostate cancers with SPOP mutations typically lack *TP53* alterations (1).

However, the K-ε-GG peptides that exhibited the most profound down-regulation coupled with robust (e.g., >2-fold) up-regulation of the corresponding total protein mapped to DEK (Fig. 1C). DEK is a putative oncoprotein, first described as a fusion gene in an aggressive subset of acute myeloid leukemia (12-14). This finding therefore raised the possibility that DEK might represent an SPOP substrate that becomes dysregulated by oncogenic prostate cancer SPOP mutations.

We next determined whether prostate cancer SPOP mutants affected DEK protein stability. Indeed, whereas forced expression of SPOP-WT in immortalized prostate epithelial cells reduced DEK protein levels, the SPOP-F133L and SPOP-Y87N mutants produced an accumulation of DEK (Fig. 1D). Treatment with the proteasome inhibitor MG132 also increased DEK, consistent with a possible role for the proteasome in DEK regulation. We also examined the effect of SPOP mutants on DEK protein stability using immortalized prostate epithelial cells engineered to express a doxycycline-inducible Flag-tagged DEK. Following doxycycline exposure, Flag-DEK decayed more rapidly in control cells than in cells containing SPOP mutants (Fig. 1E); there was no difference in DEK mRNA expression (fig. S3E). These results lent additional credence to the premise that prostate cancer SPOP mutants function in a dominant-negative fashion to impair ubiquitylation and proteasomal degradation of DEK.

Given that forced expression of SPOP reduced DEK protein levels, we sought to determine whether SPOP interacts with DEK directly to promote ubiquitylation. In support of this hypothesis, the primary DEK amino acid (AA) sequence contained a 5-AA consensus SPOP-binding motif (fig. S3F)(5). To test this, we first overexpressed a Flag-tagged DEK protein harboring serine-to-alanine mutations at the motif (S287A/S288A) and assessed the ability of wild type SPOP to repress DEK expression. As predicted, the S287A/S288A variant abolished the repressive effect of SPOP and produced elevated levels of DEK protein

(Fig. 2A). To determine if this motif mediated direct binding of SPOP to DEK, we performed immunoprecipitation experiments in cells expressing either wild type DEK or the S287A/S288A variant. Whereas overexpressed SPOP protein was detectable following immunoprecipitation of Flag-DEK (Fig. 2B) and vice versa (fig. S4A), the DEK(S287A/S288A) variant disrupted the DEK-SPOP interaction (Fig. 2B). Thus, the SPOP binding motif within DEK appeared necessary for SPOP binding and destabilization.

Next, we tested whether SPOP could ubiquitylate DEK as part of a larger CUL3-RBX1 complex(8). In vitro, the addition of CUL3 and RBX1 caused wild type DEK to migrate as high molecular weight species indicative of a multiple mono-ubiquitylation pattern (Fig. 2C, fig. S4B). In contrast, DEK(S287A/288A) failed to undergo efficient ubiquitylation (Fig. 2C). Addition of an ubiquitin moiety that is unable to form polyubiquitin chains due to lysine-to-arginine substitutions produced a similar pattern (K0, fig. S4C), thereby supporting the idea that SPOP may promote “multi-monoubiquitylation” of DEK. This result aligns well with the observation that multiple ubiquitylated DEK lysine residues were detected in the initial proteome analysis (fig. S2E).

To determine whether DEK ubiquitylation targets this protein for proteasomal degradation, we cultured SPOP- and DEK-expressing cells in the presence or absence of the proteasome inhibitor MG132. Short-term (4-5 hr) MG132 treatment markedly increased ubiquitylated Flag-DEK, with a smaller effect on total protein expression (Fig. 2D and S4D). Prolonged proteasomal inhibition (16 hr), or depletion of SPOP with two independent lentiviral shRNAs, also increased DEK protein levels (fig. S4E). Moreover, SPOP knockdown increased DEK stabilization after doxycycline removal using the inducible system described above without affecting DEK mRNA levels (figs. S4F-G). In aggregate, these data are consistent with a model in which multi-monoubiquitylation of DEK promotes its proteasomal degradation, in line with recent studies showing that multiple mono-ubiquitylation can be sufficient for proteosomal targeting (15). The lower affinity of mono-ubiquitin moieties (as opposed to ubiquitin chains) for the proteasome may explain why DEK protein turnover is relatively slow (Fig 1D, E and fig. S4F) (15).

We next asked whether prostate cancer SPOP mutations might disrupt the interaction between SPOP and DEK. Neither SPOP-F133L nor SPOP-Y87N could ubiquitylate DEK effectively in vitro (Fig. 2E). Moreover, both of these SPOP mutants suppressed ubiquitylation induced by SPOP-WT (Fig. 2E) and decreased basal DEK ubiquitylation in cell culture (fig. S5A). In prostate epithelial cells, overexpression of mutant SPOP resulted in increased total SPOP and DEK protein expression, as expected. However, both SPOP-F133L and SPOP-Y87N substantially reduced the interaction of wild-type SPOP with Flag-DEK in immunoprecipitation assays (fig. S5B). These data thus support the notion that prostate cancer SPOP mutants may impair DEK ubiquitylation in a dominant-negative manner.

Suppression of ubiquitylation by mutant SPOP may conceivably occur through heteromeric (e.g., WT/mutant) SPOP complexes. Along these lines, SPOP is known to undergo dimerization and multimerization through its BTB and BACK domains (5, 16, 17). In support of this model, Flag-tagged SPOP-F133L co-immunoprecipitated with HA-tagged

SPOP-WT (fig. S6A). To determine whether dimerization might mediate the suppressive function of SPOP-F133L, we introduced dimerization-deficient mutations involving the BTB (L186D/L190D/L193D/I217K; BTB-dd) or BACK (Y353E; BACK-dd) domains into SPOP-F133L (5, 17). Both dimerization-deficient mutants abolished formation of high molecular weight SPOP complexes and retained CUL3 binding, as evidenced by size exclusion chromatography (fig. S6B). Similarly, HA-tagged versions of these SPOP mutants showed appropriate subcellular localization, and co-immunoprecipitated with MYC-tagged CUL3 (fig. S6C and D). However, both the BTB and BACK domain mutations reversed the suppressive effect of SPOP-F133L mutant on DEK ubiquitylation in vitro (Fig. 2F) and in vivo (fig. S6E). In particular, the dimerization deficient mutations impaired the interaction of wild-type SPOP with Flag-DEK based on immunoprecipitation experiments (fig. S6F). In aggregate, these data support the notion that prostate cancer SPOP mutations exert a dominant-negative effect on wild type SPOP activity through formation of heteromeric complexes.

Next, we assessed whether DEK might contribute to oncogenic phenotypes induced by mutant SPOP in prostate cancer. Toward this end, both DEK and SPOP have previously been implicated in cell invasion (1, 18). We found that SPOP-F133L and SPOP-Y87N induced collagen invasion by prostate epithelial cells, whereas wild type SPOP suppressed invasion (Fig. 3A). Similar effects were observed in the LNCaP cells (fig. S7A). To assess the contribution of DEK to this phenotype, we over-expressed DEK in cells expressing SPOP-WT or an empty vector control, and analyzed the resulting invasion phenotypes. In both settings, DEK overexpression promoted cellular invasion (Fig. 3B). Similarly, overexpression of flag-DEK-S287A/S288A—the mutant form of DEK that cannot bind SPOP—also increased invasion, implying that this phenotype is not simply a consequence of trapped SPOP-DEK complexes (fig. S7B). Conversely, shRNA knockdown of DEK decreased cellular invasion in cells over-expressing SPOP-87N (Fig. 3B) but the effect on control cells was minimal (fig. S7C). These results suggest that DEK may influence the invasive phenotype conferred by prostate cancer SPOP mutations, although a SPOP-independent role for DEK in cellular invasion cannot be ruled out.

DEK has also been implicated in the maintenance of stem cell-like properties, such as sphere formation under non-adherent culture conditions (14, 18-20). Consistent with these observations, SPOP-Y87N produced elevated DEK levels and enhanced sphere formation in primary human prostate epithelial cells (hPREC, Fig. 3C, fig. S7D). In contrast, overexpression of SPOP-WT suppressed sphere formation in this setting (Fig. 3C, fig. S7D). Overexpression of DEK in hPREC cells also augmented sphere formation, whereas shRNA depletion of DEK (with three independent shRNAs) in cells over-expressing SPOP-87N impaired sphere-forming capacity (Fig. 3D, fig. S7D). Taken together, these data suggest that SPOP-dependent DEK regulation may promote a stem-like phenotype.

We then investigated whether the effects of SPOP mutations on DEK regulation might be generalizable across a broad spectrum of cancer-associated SPOP mutations. Here, we tested SPOP mutants from both prostate and endometrial cancer for their effects on DEK protein levels, collagen invasion, and sphere formation. All prostate cancer-associated SPOP mutants examined (representing >80% of mutations identified in this tumor type (1))

conferred increased DEK protein expression, whereas two recurrent endometrial cancer-associated SPOP mutants (S80R and E50K) (2, 3) had no effect (Fig. 4A, figs. S8A, S9A, S10A) in prostate cells. As expected, DEK expression correlated with sphere-forming capacity and cell invasion without affecting baseline cell proliferation or viability (fig. S8B, C and S9B).

Finally, we considered whether other putative SPOP effector proteins—both known substrates and novel ones nominated by our ubiquitylome screen—might also undergo dysregulated expression in the setting of prostate cancer SPOP mutations (8, 9, 21-23). Regarding the latter, we noted that TRIM24 represented another putative SPOP substrate from our screen with potential biological relevance to prostate cancer (Fig1B, C and fig. S3C) (10, 11). As expected several known or putative SPOP substrates were down-regulated in response to SPOP-WT overexpression (including DEK, TRIM24, NCOA3, DAXX, BRMS1, GLI1 and 2; Fig. 4A, fig. S10A). However, only DEK, TRIM24, and NCOA3 also became up-regulated upon overexpression of prostate cancer SPOP mutants in this setting (6). Moreover, nuclear expression of these proteins correlated significantly with SPOP mutations in 181/178 primary prostate cancers analyzed by immunohistochemistry (Fig. 4B, C and fig. S10B, table S3). These data are consistent with the ubiquitylome and experimental studies, thus supporting a model in which SPOP mutations may engage overlapping routes of transformation in prostate cancer by dysregulation of DEK, TRIM24 and NCOA3.

These data support a model wherein prostate cancer SPOP mutants impair ubiquitylation and degradation of a subset of SPOP substrates in a dominant-negative manner to promote tumorigenesis. Future studies of DEK dysregulation and its biological functions in normal and tumor tissue may therefore promote new biological insights relevant to many human cancers. More generally, large-scale profiling of the ubiquitin landscape linked to tumor genomic alterations in protein homeostasis genes may catalyze the identification of downstream effector mechanisms. Given the growing number of such genes identified by comprehensive cancer genome studies, this approach may provide an additional avenue for functional annotation of the cancer genome. In the future, these studies could uncover new biological and therapeutic avenues that exploit dysregulated protein homeostasis or ubiquitin-based regulation in cancer.

Materials and Methods

SILAC-labeling and Cell Culture

For SILAC experiments, LHMAR cells were cultured in Rosewell Park Memorial Institute (RPMI) 1640 media (custom preparation from Caisson Laboratories) deficient in L-arginine and L-lysine and supplemented with 10% dialyzed fetal bovine serum (FBS) (Sigma-Aldrich), penicillin, streptomycin, and L-glutamine (Invitrogen) and either L-arginine (Arg-0) and L-lysine (Lys-0), L-arginine [$^{13}C_6$]HCl (Arg-6) and L-lysine-4,4,5,5-d4 (Lys-4), or [$^{13}C_6$, $^{15}N_4$]HCl (Arg-10) and L-lysine [$^{13}C_6$, $^{15}N_2$]HCI(Lys-8) (Sigma-Aldrich) for 21 days (15 doublings). All media were supplemented with L-proline to prevent the conversion of arginine to proline(24). Specifically, isogenic cell lines expressing either vector control (C), wild type SPOP (SPOP-WT) or mutants (MTs) were isotopically labeled

with SILAC media and grouped into two replicates (Fig. 1A). In replicate one, cells over-expressing the most prevalent SPOP-F133L mutant were labeled with heavy medium. In the second replicate the labeling was switched to rule out labeling artifacts and another recurrent mutant was introduced (SPOP-Y87N). Approximately 100 million cells per condition were washed twice with PBS, harvested, and snap frozen.

K-ε-GG profiling and proteome analysis by liquid chromatography mass-spectrometry

Preparation of proteins for mass spectrometry analysis was completed as previously described(25). Briefly, cell pellets were lysed in an ice cold urea lysis buffer containing, 8 M urea, 50 mM Tris HCl, pH 8, 150 mM NaCl, 1 mM EDTA, 2 ug/ml aprotinin (Sigma-Aldrich), 10 mg/ml leupeptin (Roche Applied Science), 1 mM phenylmethylsulfonyl fluoride (PMSF), 50 uM PR-619, and 1 mM chloroacetamide. The lysate was cleared by centrifugation at 20,000g for 10min. A bicinchoninic acid (BCA) protein assay (Peirce) was used to determine the protein concentration of each sample. Respective SILAC mixes were created by combining 10 mg of protein per SILAC state. Proteins were reduced with 5 mM DTT at RT and subsequently alkylated with 10 mM iodoacetamide at RT in the dark. Lysates were diluted 1:4 with 50 mM Tris HCl, pH 8 and proteins were digested with sequencing grade trypsin using an enzyme to substrate ratio of 1:50, O/N at 25 C. Digests were quenched with TFA and the peptide solutions were cleared by centrifugation prior to desalting. Peptides were desalted using tC18 SepPak SPE cartridges (Waters) exactly as previously described(25).

Peptides were fractionated offline by basic pH reversed-phase (bRP) chromatography as previously described(25, 26). Briefly, dried peptides were reconstituted in bRP buffer A (5 mM ammonium formate (pH 10.0)/2% acetonitrile). A Zorbax 300 Extend-C18 column (9.4 × 250 mm, 300 A, 5 μm; Agilent) was used for the separation. Using the gradient and flow rate settings previously described(25) a total of 96 2 ml fractions were collected across the entirety of the bRP separation. For proteome analysis, 5% of each fraction was taken and combined in a non-contiguous manner such that every 22nd fraction was combined to combine 22 final fractions. For K-ε-GG analysis, the remainder of each fraction was combined in a non-contiguous manner such that every eighth fraction was combined (final fraction 1 = 1,9,17,25,33,41,49,57,65; final fraction 2 = 2,10,18,26,34,42,50,58,66) to create 8 final fractions. Pooled fractions were dried completely using vacuum centrifugation.

For enrichment of K-ε-GG peptides, anti-K-ε-GG antibody from the PTMScan ubiquitin remnant motif (K-ε-GG) kit was utilized (Cell Signaling Technology, cat. no. 5562). Prior to enrichment, the antibody was cross-linked to protein A beads using dimethyl pimelimidate (DMP)(25). Peptides were reconstituted in immunoaffinity purification (IAP) buffer and the enrichment was completed exactly as previously described(25). Briefly, peptides were incubated with approximately 31 ug of anti-K-ε-GG antibody beads and incubated for 1 h at 4 °C with rotation. Beads were washed twice with 1.5 ml of ice-cold IAP buffer followed by three washes with ice-cold PBS. K-ε-GG peptides were eluted from the antibody with 2 × 50 ul of 0.15% TFA. Peptides were desalted using StageTips. StageTips were conditioned by washing with 50 ul of 50 % MeCN/0.1% formic acid (FA) followed by 2 × 50 ul of 0.1% FA. Peptides were then loaded on StageTips, washed 2 × with 50 ul of 0.1% FA and eluted

with 50 ul of 50 % MeCN/0.1% formic acid (FA). Eluted peptides were dried completely using vacuum centrifugation.

Samples were reconstituted in 3% MeCN/0.1% FA. All samples were analyzed by nanoflow-UPLC-HCD-MS/MS using a Q Exactive mass spectrometer (Thermo Fisher Scientific) coupled online to an Easy-nLC 1000 system (Proxeon). For K-ε-GG and proteome samples, 4/8 ul and 1/20 ul were injected into the mass spectrometer, respectively. Samples were injected at a flow rate of 500 nl/min onto a PicoFrit column (360 μm (OD) × 75 μm (ID)), 10 μm ID tip, 50 cm length (New Objective) self-packed with 24 cm of ReproSil-Pur 120 A, 1.9 μm C18-AQ beads. The nanoflow column was heated to 50 °C using a column heater (Pheonix S&T). For LC-MS/MS analyses, the gradient and flow rate settings were used as previously described (25) and the MS acquisition time used for each K-ε-GG and proteome sample was 140min and 120 min, respectively. The Q Exactive was operated by acquiring an MS1 scan (R=70,000) followed by MS/MS scans (R=17,500) on the 12 most abundant ions. An MS1 and MS2 ion target of $3 \times 10^{A}6$ and $5 \times 10^{A}4$ ions, respectively was used for acquisition. A maximum ion time of 20 ms and 120 ms was used for MS1 and MS2 scans, respectively. The HCD collision energy was set to 25, the dynamic exclusion time was set to 20 s and the peptide match and isotope exclusion functions were enabled.

MS Data Analysis

K-ε-GG enriched data were processed using both the Spectrum Mill (version 4.1 beta; Agilent Technologies) and MaxQuant (version 1.2.2.5) software packages. Proteome data were processed using MaxQuant. For the MaxQuant search, the human Uniprot database including 248 common laboratory contaminants was used for searching. For the MaxQuant search, the enzyme specificity was set to trypsin, the maximum number of missed cleavages was set to 2, the precursor mass tolerance was set to 20 ppm for the first search, and the tolerance was set to 6 ppm for the main search. Carbamidomethylation of cysteines was searched as a fixed modification and oxidation of methionines and N terminal acetylation of proteins was searched as variable modifications.

For K-ε-GG data, addition of glycine-glycine to lysine was also searched as a variable modification. For identification, the minimum peptide length was set to 6, and false discovery rate for peptide, protein, and side identification was set to 1 %. The filter labeled amino acids and peptide quantification functions were enabled. For the Spectrum Mill search, MS data were searched against the identical human Uniprot database, the enzyme specificity was set to trypsin, and the maximum number of missed cleavages was set to 2. The precursor mass tolerance was set to 20 ppm and the fragment ion tolerance was set to 50 ppm. The minimum matched peak intensity was set to 30%. Similar to the MaxQuant search, carbamidomethylation of cysteines was searched as a fixed modification and oxidation of methionines, glycine-glycine addition to lysines, and N terminal acetylation of proteins was searched as a variable modifications. For the K-ε-GG data, K-ε-GG peptides identified by MaxQuant were considered for the dataset. Those MS/MS scans that were not identified in MaxQuant but were identified as a K-ε-GG modified peptide with Spectrum Mill were considered for the data set.

As previously described, to simplify K-ε-GG peptide grouping, K-ε-GG site localization information was simplified such that an original localization score of >0.75 was deemed a confidently localized site and denoted with a score of 1, an original localization score of <0.75 and >0.5 was deemed 50 % localized and denoted with a score of 0.5; and an original localization score of <0.5 was deemed unlocalized and therefore no localization score was given(27). Peptide identifications in which glycine-glycine sites were localized to a C-terminal lysine residue of a peptide were considered false positives and manually removed from the data set. Non-K-ε-GG peptides were used to normalize K-ε-GG ratios. After normalization, a median K-ε-GG log2 transformed SILAC ratios was calculated across all non-distinct forms of a K-ε-GG peptide.

For the proteome data, proteins were considered in the dataset if they were identified by 2 or more razor/unique peptides and quantified by 3 or more ratio counts in both biological replicates. K-ε-GG peptides were considered if they were quantified across both biological replicates and within each biological replicate. The SILAC ratios corresponding to the K-ε-GG site on WIZ were calculate manually due to missed identification of the peptide by the search engines in the second replicate. To address variability within a replicate across SILAC states, for each replicate, a MT/WT ratio was calculated from the measured WT/C and MT/C ratios. Residuals were calculated by subtracting the values for the calculated MT/C ratio from the measured MT/C ratio. Peptides with residual values greater than 3 standard deviations from the mean were filtered out of the dataset.

To capture ubiquitylation changes associated with protein degradation, we normalized the K-ε-GG changes to their measured protein levels. Quantitative, protein-normalized measurements were available for 7,181 replicated K-ε-GG peptides. To assess and highlight which of the significantly deregulated K-ε-GG peptides were paralleled with opposing effects on total protein expression in the MT/WT case, protein normalized K-ε-GG MT/WT SILAC ratios were multiplied by their corresponding protein level ratio and also by −1 (Fig. 1C). One data point for SECTM1 was excluded from the plot in (Fig. 1C), because of anti-correlating results across replicates.

An enrichment analysis was completed for the occurrence of previously published SPOP-binding consensus sequences “VTSTT”, “PSSSS”, “PSSTS”, “ADSTT”, “VSSST”, “VSSTS”, and “ADSST” in our dataset(5). For the analysis, all K-ε-GG modified proteins were searched for these consensus sequences (see table S2).

Cell Culture, Transfections and Lenti-Virus Production

LHMAR cells and derivate have been kindly provided by the Hahn lab (7) and primary human prostate epithelial (hPREC) cells purchased ScienCell Research Laboratories. LNCAP and PC3 cells were obtained from ATCC. LHMAR and LNCAP cells were cultured in RPMI medium, PC3 cells in DMEM supplemented with 10 % Fetal Bovine Serum (FBS) (BenchMark™) and 1 % Penicillin/Streptomycin/L-Glutamate. hPREC were cultured in F-medium supplemented with ROCK inhibitor as described(28). All cells were incubated at 37 °C and 5 % CO2. For stable shRNA knockdown pLKO-1 vectors from SIGMA were used according to the manufacturer’s protocol with culturing the cells in the presence of 2 microgram/microliter puromycin for selection of at least 3 days. For DEK knockdown, the

following clones were used: KD1 = clone TRCN0000013104 and KD2 = clone TRCN0000013105 and KD3 = TRCN0000013106. Depletion of SPOP was achieved by KD1 = TRCN0000140431 and KD2 = TRCN0000139181. The following hairpin was used as a non-silencing control: SHC002 MISSION pLKO.1-puro Non-Mammalian shRNA Control, sequence CAACAAGATGAAGAGCACCAA (referred to as Non-sil.). For over-expression a derivate of the pLX304 vector was used throughout in which the CMV promoter has been exchanged to a PGK promoter and the blastocidin cassette exchanged by mOrange (pLX_TRC_307, available at Addgene as Plasmid 41392, pCW107). All ORFs were cloned into pLX_TRC_307-mOrange using Nhe1 and Mlu1. All knockdown and overexpression experiments (with the exception of co-immunoprecipitation experiments in transiently transfected 293T cells) were performed under steady state conditions (5–14 days after infection).

Immunoblotting, Antibodies and Chemicals

Unless otherwise specified, cells were washed with PBS and lysed in RIPA buffer. Following protein normalization using the BCA reagent (Sigma), equal amounts of protein were resolved by SDS-PAGE (Life Technologies) and transferred to PVDF-Fl membranes (Bio-Rad). Western blots were blocked with Li-Cor blocking buffer and then probed with the desired antibodies overnight at 4 °C. Bands were detected using infrared fluorescence and an Odyssey scanner (Li-Cor Biosciences). The following antibodies were used to detect: VCL (4650), MYC (2272), ACTB (4967) DAXX (4533), NCOA3 (2126) all from Cell Signaling Technology and SPOP (ab81163, Abcam), hTERT (600-401-252S, Rockland Immunochemicals), large T-antigen (NB100-2755, Novus Biologicals), androgen receptor (sc-7305) and TRIM24 for immunoblotting (sc-271266) from Santa Cruz Biotechnology, DEK (610948, Bd Biosciences), Flag-tag (F1804 and F7425 Sigma-Aldrich), and HA-tag (H3663) and TRIM24 for immunohistochemistry (HPA043495) from Sigma Aldrich. To detect interactions between SPOP and Flag-DEK, cells were lysed in 1 % NP40 buffer (50mM Tris-HCl pH 7.4, 150 mM NaCl, 1 % NP40) with 2× protease inhibitor cocktail (Complete, Roche) and 3 mg of lysate were incubated overnight with 1 μg of anti-Flag-tag or control mouse IgG antibody (sc-2025, Santa Cruz Biotechnology) at 4 °C. Subsequently, antibodies were collected by 12.5 μl protein A/G magnetic beads (88803, Fisher Scientific) for 2h, followed by 2 washing steps with 1 % NP40 buffer. Proteins were eluted by addition of 1× SDS-sample buffer under reducing conditions at 95 °C for 5 min. For co-immunoprecipitation of endogenous DEK and SPOP, cells were lysed in RIPA lysis buffer and supplemented with complete protease inhibitor cocktail for 10 min. Lysates were then diluted 1:10 in 0.1% NP40 buffer (50mM Tris-HCl pH 7.4, 150 mM NaCl, 1.5 mM MgCl2, 0.1% NP40). After centrifugation at 13,200 rpm for 10 min to remove cell debris. Five μg of lysate was incubated with 3 μg of DEK antibody overnight. Antibody was collected with 12.5 μl protein A/G magnetic beads (88803, Fisher Scientific) for 2h, followed by 4 washing steps with 0.1% NP40 buffer. Proteins were eluted by addition of 1× SDS-sample buffer at 95 °C for 5 min. Quantitative analysis of the Western blots for proteins was normalized to VCL expression using infrared fluorescence and an Odyssey scanner (Li-Cor Biosciences) Biosciences. MG-132 was purchased from SIGMA and used at 10 μM in all experiments. Bortezomib and Epoximcin was purchased from SIGMA and used at the indicated

concentrations for 4h. Doxycycline was purchased from SIGMA and used at 1 μg/ml for 48h to induce Flag-DEK expression in LHMAR cells.

Immunofluorescence

For co-localization studies of mutant and wild-type SPOP, 293T cells were sparsely seeded in a 96-well clear bottom plate and transfected the next day with 15ng of flag-SPOP-WT and 15ng of HA-SPOP-mutant construct as indicated in fig. S5C. Two days later, cells were washed twice with PBS and fixed for 5 min with ice-cold methanol. Next, cells were incubated with Li-Cor blocking buffer with a 1:1000 dilution of anti-HA (mouse) and anti-Flag (rabbit) antibody and incubated for 2h at room temperature. After two washing steps, cells were then incubated with anti-rabbit (Anti-Rabbit Alexa Fluor® 594, ab150092) and anti-mouse (Anti-Mouse Alexa Fluor® 488, ab150113) antibodies at a dilution of 1:1000 for another 2h. Finally, cells washed again 3 times with PBS and nuclei stained with DAPI.

In Vitro Ubiquitylation

Wild-type and SPOP-binding mutant (SB) constructs of FLAG-tagged human DEK were purified from stably transfected LHMAR cells maintained in RPMI 1640 media (Sigma). Human SPOP was expressed and purified from *E. coli* as described previously(16). SPOP mutations were engineered using the QuikChange (Agilent) method of site-directed mutagenesis. Recombinant human His_6-UbcH5b and Thx-His_6-Puc^{1-381} were expressed and purified from *E. coli* by Ni-NTA and size-exclusion chromatography. In vitro ubiquitylation reactions were assembled as follows. For each 20 μl reaction, ~10^7 FLAG-DEK-expressing LHMAR cells were harvested and lysed by sonication in IP buffer (20 mM Tris-Cl pH 7.4, 150 mM NaCl, 5% glycerol, 1 mM TCEP, 1× Roche protease inhibitor cocktail). Immunoprecipitates were prepared with 10 μL of anti-FLAG M2 affinity gel (Sigma) and washed with IP buffer. To each FLAG-DEK immunoprecipitate was added 2 μM SPOP, 1 pM Cul3/Rbx1 (Ubiquigent), 500 nM UbcH5b, 200 nM Uba1 (BostonBiochem), 50 μM wt or K0 ubiquitin (BostonBiochem), 5 mM ATP, 10 mM MgCh, 150 mM NaCl, 20 mM Tris-Cl pH 7.4, 1 mM TCEP and 1× protease inhibitor cocktail. To assess the effect of SPOP dimer-defective (SPOP-dd) mutants on SPOP wt E3 ubiquitin ligase activity, 2 μM SPOP wt was pre-incubated with 2 μM of the indicated SPOP-dd for 30 minutes at 30°C. 4 uM of the SPOP-wt/dd mixture was then used in the above reaction scheme. Reactions were incubated with mixing at 30°C for 180 minutes (or other indicated time points). Reactions were stopped by isolating the anti-FLAG IP, washing with IP buffer, followed by the addition of SDS sample buffer. Samples were separated by SDS-PAGE and visualized using anti-FLAG (Sigma; F7425) and infrared fluorescence and an Odyssey scanner (Li-Cor Biosciences).

Analytical Size-Exclusion Chromatography

SPOP and Cul3 proteins were prepared as described previously(16). All proteins were prepared in SEC buffer (20 mM Tris-Cl pH 7.4, 150 mM NaCl, 1 mM TCEP) and brought to a final concentration of 30 μM in Amicon Ultra centrifugal filters (Millipore). 2 nmoles of each protein (either alone or mixed in the indicated complex) were injected onto a KW-804 SEC column (Shodex), which was run in SEC buffer at a flow rate of 1 ml/min and monitored by UV absorbance at a wavelength of 280 nm.

In Vivo Ubiquitylation

For in vivo ubiquitylation 2.4 Mio 293T cells were seeded and transiently transfected the next day with the following plasmids as indicated in Fig. 2 and fig. S4D: pCW107-flag-DEK or pCW107-flag-DEK-S287A/S288A (1.5 μg), pCW107-SPOP-WT or -MT (1.5 μg), pcDNA3-MYC-RBX1 (1.5 μg) and pcDNA3-MYC-CUL3 (1.5 μg), CMV-8xHis-Ub (1.5 μg). Empty vector pCW107 was used to bring the total plasmid DNA to 9 μg for each transfection. Two to three days later, cells were treated with MG132 (10 μM) or DMSO for additional 5 hours. The cells were then washed twice with ice cold PBS, scraped off the plates in PBS and then collected by centrifugation. A small aliquot of the cells was lysed in RIPA buffer, and the rest were lysed in Buffer C (6M guanidine-HCL, 0.1M Na2HPO4/NaH2PO4, 10 mM imidazole, pH 8.0). After sonication, the whole cell extract were mixed with 100 μL of Ni-NTA agarose magnetic beads at 4 degree Celsius overnight. Next, the Ni-NTA beads were washed twice with Buffer C, twice with Buffer D (1 Volume of Buffer C: 3 volumes of Buffer E), and once with Buffer E (25 mM Tris.CL, 20 mM imidazole, pH 6.8). Bound proteins were then eluted by boiling in 1× SDS loading buffer containing 300 mM imidazole, resolved by SDS polyacrylamide gel electrophoresis, and detected by immunoblot analysis.

Quantitative PCR experiments

Samples were processed using the RNeasy Mini Kit (Qiagen) according to manufacturer's procedure. Obtained RNA was transcribed into cDNA by applying the You-Prime-First-Strand Beads kit (GE Healthcare) using random hexamer primers. PCR reactions were carried out on a Roche Light Cycler Lc480. For the housekeeping GAPDH the following primers were used: ACACCATGTATTCCGGGTCAAT (forward) and TGTGGGCATCAATGGATTTGG (reverse) at an annealing temperature of 55 °C. The primer set for DEK was purchased (sc-38253-PR, Santa Cruz Biotechnology).

Clonogenic, Invasion and Sphere Formation Assays

For clonogenic assays, LHmAr cells were seeded at 1000 cells/well in 12-well plates (NUNC) and grown for 7 days. Plates were fixed and stained using Giemsa's azur eosin methylene blue (MERCK), diluted 1:1 in 100 % methanol. Staining was re-suspended in 10 % acetic acid and the OD at 560 nm measured for quantification purposes. The ability of cells to invade collagen was measured using the colorimetric QCM™ Collagen Cell Invasion Assay (ECM551, EMD Millipore) according to the manufactures instructions. Cells were starved in serum free media for 24 h before seeding at a density of 250'000 cells per chamber and incubated with and without serum for an additional 24 h. The cells at the outer side of the chamber were stained, lysed and quantified by measuring the OD at 560 nm. Primary prostate epithelial cells (hPRECs) were cultured for five passages in standard prostate epithelial medium (PEpiCM, ScienCell Research Laboratories) and frozen down. Subsequently, hPRECs were thawed and cultured in F-medium with Rho-kinase inhibitor(28) for immunoblotting and diluted to single cells to 1×10^5 cell/ml in PrEGFM sphere medium as described(29) and 40 microliter of cells mixed with 60 microliter of cold Matrigel (BD Matrigel™). The mixture was subsequently pipetted around the rim of a 12-well plate, swirled and incubated at 37 degree Celsius CO_2 for 30min(29). After adding 1ml

of PrEGFM medium to the well, cells were incubated at 37 degree Celsius CO_2 for 10d with medium changes every 3 days. Spheres with a size over 40 micrometers were counted (29).

Human Tumor Samples

We assessed 251-selected primary prostate tumors for the presence of prostate-specific *SPOP* mutations by high resolution melt analysis assay followed Sanger sequencing of exon 6 and 7 (4). Due to tissue loss (a common problem encountered with tissue microarrays out of the 251 samples 181 were histologically analyzable. These tumors represent are part of tissue microarrays composed of paraffin-embedded prostate tissue cores from two different institutes of pathology. As previously published, specimens were collected between 1993 and 2007 from the Institute of Surgical Pathology, University of Zurich, Switzerland, and the Institute of Pathology, University of Regensburg, Germany (30). The local scientific ethics committees approved both cohorts (approval no.: StV-Nr. 25/2007). See table S3 for details on SPOP mutations.

Immunohistochemistry

For the detection of dEk, slides were analyzed with the Bond-III automated staining system (Leica) using manufacture reagents for the entire procedure. For antigen retrieval, slides were incubated using program H2 for 45 min. For NCOA3 and TRIM24, slides were analyzed with the Ventana Benchmark automated staining system (Ventana Medical Systems). For antigen retrieval, slides were incubated using program CC1 for 1 h (Tris-based buffer with slightly alkaline pH). Thereafter, slides were incubated with the primary antibodies at following concentrations: DEK (1:400) and NCOA3/TRIM24 (1:300) for 1 h. Detections were performed for DEK using the detection refine 30/30 kit (Leica) and for NCOA3 the UltraMap-Rabbit-DAB system (Ventana Medical Systems). Immunohistochemical staining was evaluated as follows for DEK and NCOA3: No detectable staining in more than 70% of tumor cell nuclei was referred as negative, 30% or more tumor cell nuclei weakly stained (discernable nucleoli) as weak and more than 30% of nuclei strongly stained (invisible nucleoli) as strong.

Statistical Analysis

A two-tailed independent Student's t test with unequal variance assumption was performed to analyze the results of cell culture experiments. Kendall beta-tau was used to test correlation of immunohistochemical staining with SPOP mutation status. Differences in the prevalence of SPOP binding sites in proteins measured by MS were assessed by Chi Square statistics. For correlation of proteome expression data by mass-spectrometry Pearson correlation coefficient was used. Statistical differences across isogenic cell lines in flag-DEK protein decay were assessed using Friedman's Two-Way Analysis of Variance by Ranks.

Supplementary Material

Refer to Web version on PubMed Central for supplementary material.

Acknowledgments

We thank Leslie Gaffney for illustrations, and Andre Fitsche and Martina Storz for excellent technical assistance. J.P.T. is funded by a fellowship from the Swiss Science foundation (SSMBS PASMP3_145764). P.J.W. is funded by a SystemX.ch grant (PhophoNet PPM), the Swiss initiative in systems biology. M.A.R. and Cornell University have filed a patent (WO 2012115789 A2) relating to the use of SPOP mutations as markers for human prostate cancer. L.A.G. is a paid consultant for the following pharmaceutical companies: Novartis Foundation Medicine, Boehringer Ingelheim, and Millennium/Takeda.

References

1. Barbieri CE, et al. Nature genetics. Jun.2012 44:685. [PubMed: 22610119]
2. Le Gallo M, et al. Nature genetics. Dec.2012 44:1310. [PubMed: 23104009]
3. N. Cancer Genome Atlas Research. et al. Nature. May 2.2013 497:67. [PubMed: 23636398]
4. Blattner ML, et al. Neoplasia. Jan 16.2014 16:1. [PubMed: 24563615]
5. Zhuang M, et al. Molecular cell. Oct 9.2009 36:39. [PubMed: 19818708]
6. Geng C, et al. Proceedings of the National Academy of Sciences of the United States of America. Apr 23.2013 110:6997. [PubMed: 23559371]
7. Berger R, et al. Cancer research. Dec 15.2004 64:8867. [PubMed: 15604246]
8. Kwon JE, et al. The Journal of biological chemistry. May 5.2006 281:12664. [PubMed: 16524876]
9. Li C, et al. Oncogene. Oct 20.2011 30:4350. [PubMed: 21577200]
10. Allton K, et al. Proceedings of the National Academy of Sciences of the United States of America. Jul 14.2009 106:11612. [PubMed: 19556538]
11. Kikuchi M, et al. Biochimica et biophysica acta. Dec.2009 1793:1828. [PubMed: 19909775]
12. von Lindern M, et al. Molecular and cellular biology. Apr.1992 12:1687. [PubMed: 1549122]
13. Riveiro-Falkenbach E, et al. Clinical cancer research : an official journal of the American Association for Cancer Research. Jun 1.2010 16:2932. [PubMed: 20501624]
14. Privette Vinnedge LM, et al. Cell cycle. Jan 1.2013 12:51. [PubMed: 23255114]
15. Kravtsova-Ivantsiv Y, Ciechanover A. Journal of cell science. Feb 1.2012 125:539. [PubMed: 22389393]
16. Errington WJ, et al. Structure. Jul 3.2012 20:1141. [PubMed: 22632832]
17. van Geersdaele LK, et al. Acta crystallographica. Section D, Biological crystallography. Sep 1.2013 69:1677.
18. Privette Vinnedge LM, et al. Oncogene. Jun 16.2011 30:2741. [PubMed: 21317931]
19. Cheung TH, et al. Nature. Feb 23.2012 482:524. [PubMed: 22358842]
20. Broxmeyer HE, et al. Stem cells and development. Jun 10.2012 21:1449. [PubMed: 21943234]
21. Zhang Q, et al. Proceedings of the National Academy of Sciences of the United States of America. Dec 15.2009 106:21191. [PubMed: 19955409]
22. Li G, et al. Cancer cell. Apr 14.2014 25:455. [PubMed: 24656772]
23. An J, et al. Cell reports. Feb 27.2014 6:657. [PubMed: 24508459]
24. Bendall SC, et al. Molecular & cellular proteomics : MCP. Sep.2008 7:1587. [PubMed: 18487603]
25. Udeshi ND, et al. Nature protocols. Oct.2013 8:1950.
26. Mertins P, et al. Nature methods. Jul.2013 10:634. [PubMed: 23749302]
27. Udeshi ND, et al. Molecular & cellular proteomics: MCP. May.2012 11:148. [PubMed: 22505724]
28. Liu X, et al. The American journal of pathology. Feb.2012 180:599. [PubMed: 22189618]
29. Guo C, et al. Methods in molecular biology. 2012; 879:315. B. [PubMed: 22610567]
30. Mortezavi A, et al. Clinical cancer research : an official journal of the American Association for Cancer Research. Mar 1.2011 17:1111. [PubMed: 21220479]

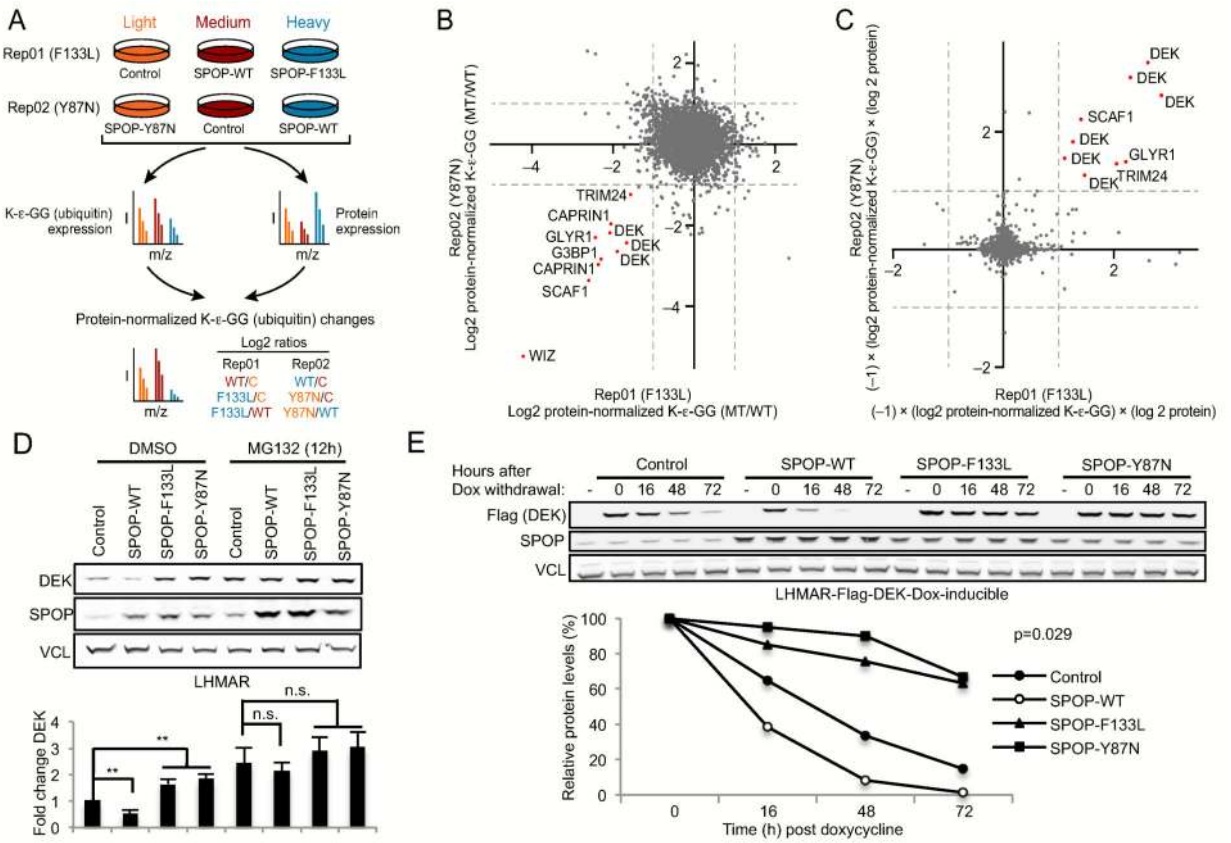

Fig. 1.

K-ε-GG (ubiquitin)-profiling and validation for DEK in immortalized prostate epithelial cells (LHMAR) over-expressing vector control, SPOP-wild-type (WT) and -F133L/Y87N mutants (MT). (**A**) Schematic showing the design of the proteomics experiments. Isogenic cell line expressing either vector control, SPOP-WT or SPOP-MT were isotopically labeled (see fig. S1A, B). K-ε-GG ratios were normalized to protein expression changes, assessed in parallel. (**B**) Scatter plot of protein normalized K-ε-GG level changes between SPOP-MT and SPOP-WT (depicted as log2 ratio of MT/WT) shows coordinate down-regulation of distinct K-ε-GG peptides across replicates (see also fig. S1C, D and S2A-G). (**C**) To visualize K-ε-GG sites that undergo inverse changes at the protein level (e.g., >2-fold), normalized K-ε-GG data shown in (B) was inverted and multiplied by corresponding total protein expression changes (see also fig. S3C, D for expression changes). (**D**) DEK protein expression across isogenic LHMAR cells assessed by immunoblotting with and without proteasome inhibition by MG132. Error bars represent mean ± SD, n=4 (n.s., not significant, **p < 0.01, Student's t test). (**E**) Degradation of Flag-DEK over time. Flag-DEK was induced by doxycycline (Dox) and protein decay measured by immunoblotting after doxycycline withdrawal in inducible LHMAR cells (p-value, Friedman test). See also fig. S3E for DEK mRNA expression.

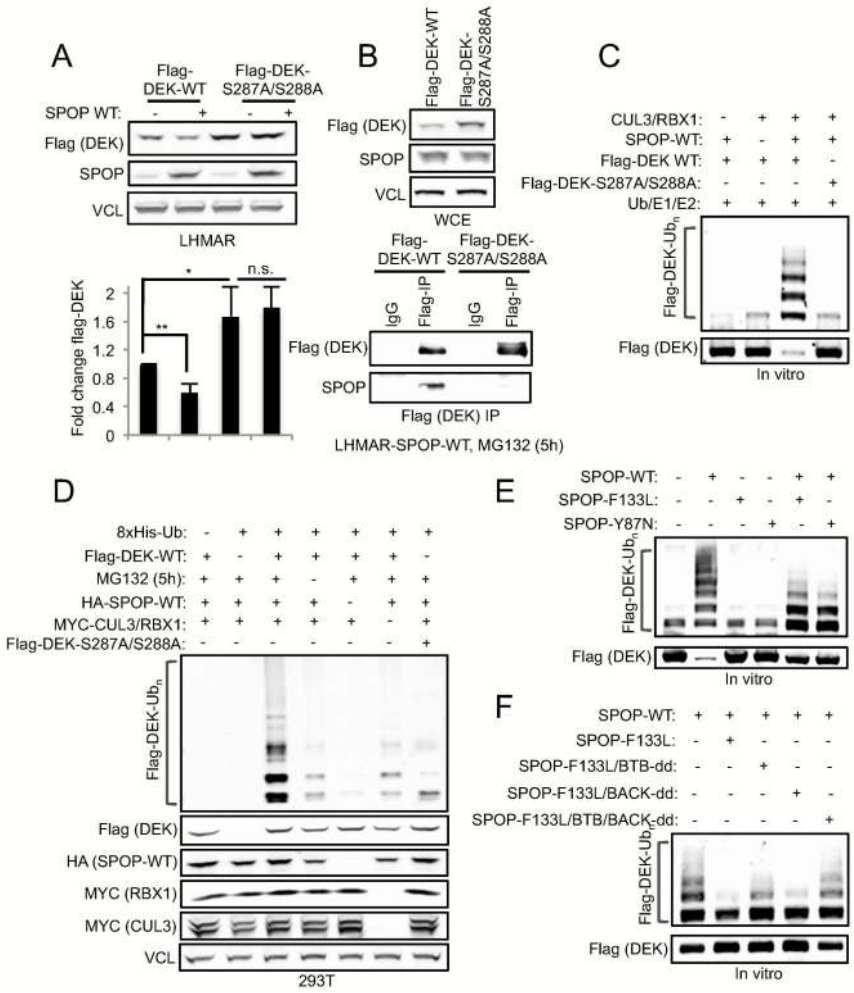

Fig. 2.

DEK is a SPOP substrate and SPOP mutants repress DEK ubiquitylation. (**A**) Effects of stable transduced wild type SPOP overexpression on protein levels of Flag-DEK and corresponding S287A/S288A mutant were assessed by immunoblotting in LHMAR cells. Error bars represent mean ± SD, n=4 (n.s., not significant, *$p < 0.05$, **$p < 0.01$, Student's t test). (**B**) Flag-immunoprecipitation of Flag-DEK and corresponding S287A/S288A mutant in LHMAR cells with forced SPOP expression. (**C**) In vitro ubiquitylation of DEK. Flag-DEK was purified by anti-Flag immunoprecipation from LHMAR cells and incubated with the indicated components. Flag-DEK immunoprecipitates were analyzed by immunoblotting (see also fig. S4B). (**D**) In vivo ubiquitylation of DEK. 293T were transfected with 8×His-Ubiquitin (Ub) and indicated constructs +/− MG132 and lysed. Immunoblot of protein lysates and 8×His-ubiquitin pull down using nickel beads. (**E**) In vitro ubiquitylation as in (C) using indicated recombinant SPOP components in equimolar ratios. See also fig. S5A. (**F**) In vitro ubiquitylation as in (E) using indicated recombinant SPOP components. Dimerization-deficient mutants of SPOP-F133L: BTB domain (L186D/L190D/L193D/I217K = BTB-dd) and BACK domain (Y353E = BACK-dd). See also fig. S6.

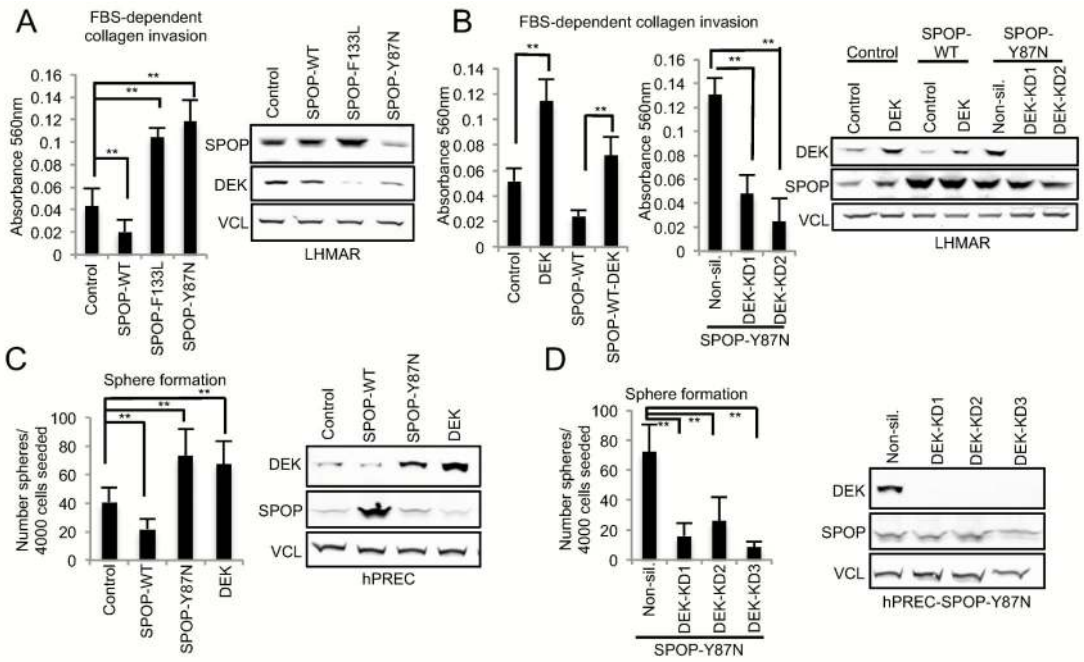

Fig. 3.

SPOP mutant-related changes in DEK expression contribute to invasion and sphere formation. (**A**) Effects of different SPOP species on collagen invasion and DEK expression in LHMAR cells. (**B**) Collagen invasion changes related to forced expression and depletion of DEK with two shRNAs in LHMAR cells. See also fig. S7. (**C**). Effects of different SPOP species and DEK on sphere formation in primary prostate epithelial cells (hPREC). (**D**) Effects of DEK depletion by three shRNAs on sphere formation Error bars represent mean ± SD, n=3 in triplicate (n.s., not significant, **p < 0.01, Student's t test). See also fig. S7D.

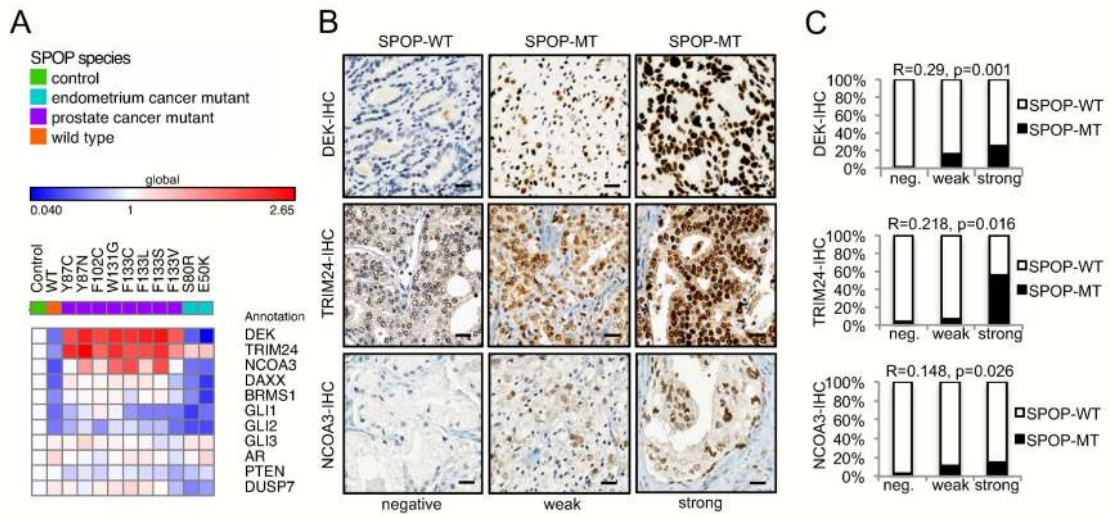

Fig. 4.

Up-regulation of DEK, TRIM24 and NCOA3 is a feature of prostate cancer SPOP mutations. (**A**) Effects of different SPOP species on abundance of indicated proteins in unmodified primary prostate epithelial cells (hPREC) by immunoblotting. Protein changes relative to individual controls depicted as median in a heatmap (n=3). (**B**) Representative images of primary prostate cancer tissues stained for DEK, TRIM24 and NCOA3 by immunohistochemistry (bar = 30 μm). (**C**) Corresponding expression analysis on 181/178 primary tumors stratified according to their SPOP mutations status (p-values, Kendall beta-tau). See also fig. S8-10.